Modern Physics Letters A
2050215 (17 pages)

DOI: 10.1142/S0217732320502156

Stability of asymmetric thin shell wormhole with a variable equation of state

A. Eid

Department of Physics, College of Science, Imam Mohammad Ibn Saud Islamic University (IMSIU), Riyadh, KSA
Department of Astronomy, Faculty of Science, Cairo University, Giza, Egypt
amaid@imamu.edu.sa

Received 27 March 2020
Revised 28 May 2020
Accepted 29 May 2020
Published 30 June 2020

Dynamical equations of asymmetric thin shell wormholes connecting two different spacetimes by applying the cut and paste technique are constructed. The linear stability with variable modified generalized Chaplygin gas (VMGCG) equation of state, where the pressure will be a function of both radius and density, is investigated. This formalism is applied to two specific cases of asymmetric wormhole of a Schwarzschild connected to Reissner–Nordström spacetime and Reissner–Nordström connected to Schwarzschild–De Sitter (SDS) spacetime.

Keywords: Astrophysics; stability; exotic matter; asymmetry thin shell wormhole.

1. Introduction

In 1966, Israel[1] provided a concrete formalism to describe spacetime junction conditions for constructing the space-like, time-like and null shells, by gluing two similar or different manifolds at the location of the thin shell. Morris and Thorne[2] investigated the traversable wormholes with a throat as a geometrical object, like tunnels that connect any two spacetimes similar or different. The formation of wormholes required an exotic matter to violate the energy conditions.[3] Visser[4] introduced the idea of thin shell wormholes (TSWs) by using the cut and paste techniques which applied to a vast variety of spacetime. Moreover, Poisson and Visser[6] analyzed the TSWs by pasting together two copies of the Schwarzschild solution. Gerica *et al.*[7] discussed generic spherically symmetric TSWs in general relativity.

The symmetric spherical and cylindrical TSWs and their stability with a different equation of state (EoS) have been studied by several researchers. Eiroa[5] discussed the TSWs with a generalized Chaplygin gas. Mazharimousavi *et al.*[8]

investigated the stability of generic cylindrical TSWs. Mazharimousavi *et al.*[9] discussed the stability of spherically symmetric time-like thin shells with a variable equation of state. Also, Varela[10] studied the linearized stability of Schwarzschild TSWs with variable EoS. Eid[11] studied the charged shell supported by phantom energy. Sharif and Azam[12] discussed the stability of the cylindrical and spherically symmetric TSWs in Newtonian and post-Newtonian approximations. Eiroa and Simeone[13] studied the cylindrical TSWs in cosmic strings. Eid[14] analyzed the cylindrical TSWs supported by phantom energy. Furthermore, thin shell wormholes supported by Chaplygin gas, phantom energy, quintessence, dissipative matter fluid, generalized Chaplygin gas, K-essence, Bulk viscous fluid have been discussed clearly.[15–20] Wang and Meng[21] investigated a new work on the thin-shell wormholes constrained by cosmological observations.

Asymmetric TSWs with different spacetimes on the two sides of the throat recently analyzed with their stabilities as well. Forghani *et al.*[22] studied asymmetric thin shell wormholes (ATSW) and their stability, and discussed the fate of a thin shell wormhole powered by Morris–Thorne wormhole.[23] Also, they analyzed the discontinuity problem in the linear stability analysis of thin shell wormholes.[24] Eventually, they extended their study to examine the stability of asymmetric cylindrical TSWs.[25]

From this perspective, it is well known that the stability of ATSWs with variable modified generalized Chaplygin gas (VMGCG) equation of state has been performed in two different cases of ATSW connecting two manifolds such that the Schwarzschild metric as connected to Reissner–Nordström spacetimes and the Reissner–Nordström metric as connected to the Schwarzschild–De Sitter spacetime. In Sec. 2, dynamics of ATSW is briefly discussed. The outline of general linearized stability about the static solution of ATSWs in two examples of Schwarzschild connected to Reissner –Nordström spacetime and Reissner–Nordström connected to Schwarzschild–De Sitter spacetime is given in Sec. 3. Finally, a remarking conclusion is presented in Sec. 4.

2. Dynamics of Asymmetric Thin Shell Wormholes

The outside and inside metric forms of the two spacetime geometries connected by ATSW are described by

$$ds_{\pm}^2 = -f_{\pm}(r_{\pm})dt_{\pm}^2 + f_{\pm}^{-1}(r_{\pm})dr_{\pm}^2 + h_{\pm}(r_{\pm})d\Omega_{\pm}^2, \tag{1}$$

where $f_{\pm}$ and $h_{\pm}$ are functions of radial coordinates $r_{\pm}$ and $\Omega_{\pm} = d\theta_{\pm}^2 + \sin^2\theta_{\pm}\, d\phi_{\pm}^2$ are unit two spheres line elements. Let $h_+ = h_- = r^2$ at the location of the throat, and the time evolution $R(\tau)$ of the shell is described by the equation $r_{\pm} = R_{\pm}(\tau)$. The induced metric on Σ (the throat) is given by

$$ds^2 = -d\tau^2 + R^2(\tau)d\Omega^2, \tag{2}$$

with a proper time τ of the shell. However, using the Darmois–Israel formalism,[1] the extrinsic curvature is defined by

$$K_{ij}^{\pm} = -n_{\gamma}^{\pm}\left(\frac{\partial^2 x^{\gamma}}{\partial\xi^i\partial\xi^j} + \Gamma^{\gamma}_{\alpha\beta}\frac{\partial x^{\alpha}}{\partial\xi^i}\frac{\partial x^{\beta}}{\partial\xi^j}\right)\vdots_{\Sigma}, \tag{3}$$

where $n_{\gamma}^{\pm}$ is the four-vector unit normal. Thus, the surface stress–energy tensor on the throat, $t_j^i = \text{diag}(-\sigma, p_\theta, p_\phi)$, of p and σ is being defined as the pressure and surface energy density, respectively, while the Lanczos equations are given by

$$t_{ij} = \frac{-1}{8\pi}([K_{ij}] - [K]g_{ij}), \tag{4}$$

where $[K]$ is the trace of $[K_{ij}] = K_{ij}^{+} - K_{ij}^{-}$. The Lanczos equations become

$$\sigma = \frac{-1}{4\pi}[K_{\theta}^{\theta}], \tag{5}$$

$$p = p_\theta = p_\phi = \frac{1}{8\pi}([K_{\tau}^{\tau}] + [K_{\theta}^{\theta}]). \tag{6}$$

Accordingly, Eqs. (5) and (6) become

$$\sigma = \frac{-1}{4\pi R}\left(\sqrt{f_+ + \dot{R}^2} - \sqrt{f_- + \dot{R}^2}\right), \tag{7}$$

$$p = \frac{1}{16\pi}\left(\frac{2\ddot{R} + f'_+}{\sqrt{f_+ + \dot{R}^2}} - \frac{2\ddot{R} + f'_-}{\sqrt{f_- + \dot{R}^2}}\right) - \frac{1}{2}\sigma, \tag{8}$$

where a "prime" and a "dot" stand for the derivatives concerning R and τ, respectively. Also, the dynamical equation of motion, derived from Eq. (7), becomes

$$\dot{R}^2 + V(R) = 0, \tag{9}$$

where the effective potential $V(R)$ is given by

$$V(R) = \frac{1}{2}(f_+ + f_-) - \frac{(f_+ - f_-)^2}{(8\pi R)^2\sigma^2} - (2\pi R)^2\sigma^2. \tag{10}$$

The energy conservation is defined by

$$\frac{d}{d\tau}\sigma = -\frac{2}{R}(\sigma + p)\frac{dR}{d\tau}, \tag{11}$$

and may be written in the form

$$\sigma' = \frac{-2}{R}(\sigma + p). \tag{12}$$

3. Stability of ATSWs with a Variable Modified Chaplygin Gas EoS

The variable modified Chaplygin gas equation of state of the throat is given by

$$p(\sigma, R) = A\sigma - \frac{B}{R^n \sigma^\alpha}, \tag{13}$$

where$B > 0$, $0 < \alpha \leq 1$, $A < 0$ and n are constants. It is reduced to a modified Chaplygin gas when $n = 0$. Since $p = p(\sigma, R)$, then its derivative becomes

$$p' = \frac{\partial p}{\partial \sigma}\sigma' + \frac{\partial p}{\partial R} \equiv \beta^2 \sigma' - \chi, \tag{14}$$

where β^2 and χ are the partial derivatives of p with respect to σ and R, respectively. Insert Eq. (13) into (12) to get

$$\sigma' = \frac{-2}{R}\left[(A+1)\sigma - \frac{B}{R^n \sigma^\alpha}\right]. \tag{15}$$

The second derivative becomes

$$(R\sigma)'' = \frac{2}{R}[(\sigma + p)(2\beta^2 + 1) + \chi R]. \tag{16}$$

Equation (16) can be expressed in terms of EoS

$$(R\sigma)'' = -(2A+1)\sigma' - 2B\left[\frac{n}{R^{n+1}\sigma^\alpha} + \frac{\alpha}{R^n \sigma^{\alpha+1}}\right]. \tag{17}$$

The solution of Eq. (15) is

$$\sigma^{\alpha+1} = \frac{2B(\alpha+1)[R^{2b}R_{\rm o}^n - R^n R_{\rm o}^{2b}] + (2b-n)\sigma_{\rm o}^{\alpha+1} R^n R_{\rm o}^{n+2b}}{R^{n+2b}R_{\rm o}^n(2b-n)}, \tag{18}$$

with $b = (A+1)(\alpha+1)$. The Taylor expansion of $V(R)$ up to second-order about $R_{\rm o}$ is given by

$$V(R) = \sum_{n=0}^{2} b_n (R - R_{\rm o})^n, \quad b_n = \frac{V^{(n)}(R_{\rm o})}{n!}. \tag{19}$$

The static solutions at $R = R_{\rm o}$ require $V(R_{\rm o}) = 0$ and $V'(R_{\rm o}) = 0$. Yet it may give rise to find out that

$$\dot{R}^2 = -V(R) = -\frac{1}{2}V''(R_{\rm o})(R - R_{\rm o})^2.$$

Consequently, using Eqs. (7), (8) and (13), one finds out that the dynamical evolution becomes

$$-2R^n \ddot{R}\left(\sqrt{f_+ + \dot{R}^2} - \sqrt{f_- + \dot{R}^2}\right)^{\alpha+1} + R^n \left(\sqrt{f_+ + \dot{R}^2} - \sqrt{f_- + \dot{R}^2}\right)^{\alpha}$$
$$\times \left(f'_+ \sqrt{f_- + \dot{R}^2} - f'_- \sqrt{f_+ + \dot{R}^2}\right)$$

$$+2R^{n-1}(2A+1)\left(\sqrt{f_+ + \dot{R}^2} - \sqrt{f_- + \dot{R}^2}\right)^{\alpha+1}$$
$$\times \sqrt{f_+ + \dot{R}^2}\sqrt{f_- + \dot{R}^2} + 16\pi B(-4\pi R)^{\alpha}\sqrt{f_+ + \dot{R}^2}\sqrt{f_- + \dot{R}^2} = 0. \quad (20)$$

Meanwhile, Eq. (20) of the static solution obtained by taking, $\ddot{R} = \dot{R} = 0$ becomes

$$R^n\left(\sqrt{f_+} - \sqrt{f_-}\right)^{\alpha}\left(f'_+\sqrt{f_-} - f'_-\sqrt{f_+}\right) + 2R^{n-1}(2A+1)\left(\sqrt{f_+} - \sqrt{f_-}\right)^{\alpha+1}$$
$$\times \sqrt{f_+}\sqrt{f_-} + 16\pi B(-4\pi R)^{\alpha}\sqrt{f_+}\sqrt{f_-} = 0. \quad (21)$$

Thus, the second derivative of Eq. (10) takes the following form:

$$V''(R) = \frac{1}{2}\Delta'' + \frac{2}{(8\pi)^2(R\sigma)^4}\Bigg\{-\frac{1}{2}\delta''(R\sigma)^2 + 2\delta'(R\sigma)(R\sigma)'$$
$$+ (R\sigma)(R\sigma)''[\delta - (16\pi^2)^2(R\sigma)^4] - (R\sigma)'^2[3\delta + (16\pi^2)^2(R\sigma)^4]\Bigg\}, \quad (22)$$

where $\Delta = f_+ + f_-$, $\delta = (f_+ - f_-)^2$. From Eqs. (13), (15) and (17), Eq. (22) becomes

$$V''(R) = \frac{1}{2}\Delta'' + 8\pi^2\Bigg\{(8A^2 + 10A + 3)\sigma^2 + \frac{4B^2}{R^{2n}\sigma^{2\alpha}}$$
$$- \frac{2B\sigma}{R^n\sigma^{\alpha}}[n + \alpha R\sigma^{-1} + 3(2A+1)]\Bigg\} + \frac{1}{32\pi^2R^4\sigma^4}\Bigg\{-\frac{1}{2}(R\sigma)^2\delta''$$
$$+ 2R\sigma\delta'\left[\frac{2B}{R^n\sigma^{\alpha}} - (2A+1)\sigma\right] + \sigma\delta\Bigg[-(8A^2 + 6A + 5)\sigma$$
$$- \frac{12B^2}{R^{2n}\sigma^{2\alpha+1}} + \frac{10B(2A+1)}{R^n\sigma^{\alpha}} - \frac{2B}{R^n\sigma^{\alpha+1}}(n\sigma + \alpha R)\Bigg]\Bigg\}. \quad (23)$$

Furthermore, rewriting Eq. (22) in terms of Eq. (16), we may obtain

$$V''(R) = \frac{1}{2}\Delta'' + \frac{1}{(8\pi)^2(R\sigma)^4}\{-\delta''(R\sigma)^2 - 4\delta'R\sigma(\sigma + 2p)$$
$$+ 4\sigma[\delta - (16\pi^2)^2(R\sigma)^4][(\sigma + p)(2\beta^2 + 1) + 2\chi]$$
$$- 2(\sigma + 2p)^2[3\delta + (16\pi^2)^2(R\sigma)^4]\}, \quad (24)$$

where β^2 is called the square of sound speed. The ATSWs are stable if $V''(R_o) > 0$, but ATSWs are unstable if $V''(R_o) < 0$. From Eq. (24), assuming $V''(R_o) = 0$, the squared sound speedβ^2 takes the following form:

$$\beta^2 = -\frac{1}{2} - \frac{\chi R}{2(\sigma + p)} + \frac{1}{8\sigma(\sigma + p)[\delta - (16\pi^2)^2(R\sigma)^4]}\Bigg\{-\frac{1}{2}(8\pi)^2(R\sigma)^4\Delta''$$
$$+ \delta''(R\sigma)^2 + 4\delta'R\sigma(\sigma + 2p) + 2(\sigma + 2p)^2[3\delta + (16\pi^2)^2(R\sigma)^4]\Bigg\}. \quad (25)$$

Moreover, substituting Eq. (13) into (24), we get

$$\beta^2 = -\frac{1}{2} - \frac{\chi R^{n+1}\sigma^{\alpha}}{2[(A+1)R^n\sigma^{\alpha+1} - B]} + \frac{R^n\sigma^{\alpha-1}}{4[(A+1)R^n\sigma^{\alpha+1} - B][4(8\pi^2)^2(R\sigma)^4 - \delta]}$$
$$\times \left\{(4\pi)^2(R\sigma)^4\Delta'' - \frac{1}{2}\delta''(R\sigma)^2 - 2\delta' R^{1-n}\sigma^{1-\alpha}[(2A+1)R^n\sigma^{\alpha+1} - 2B]\right.$$
$$\left. - [4(8\pi^2)^2(R\sigma)^4 + 3\delta][(2A+1)R^n\sigma^{\alpha+1} - 2B]^2 R^{-2n}\sigma^{-2\alpha}\right\}. \quad (26)$$

3.1. *For a Schwarzschild and Reissner–Nordström Spacetimes*

In case of RN spacetime, the metric $f_{\pm}$ of the line element (1) is given by

$$f_{\pm}(r_{\pm}) = 1 - \frac{2m_{\pm}}{r_{\pm}} + \frac{q_{\pm}^2}{r_{\pm}^2}, \quad (27)$$

where $m_{\pm}$ are the gravitational masses and $q_{\pm}$ are the charges of two spacetimes. In the case of Schwarzschild and RN spacetimes assuming that: $m_- = m$, $m_+ = (1+\zeta)m$, $q_- = 0$ and $q_+ = q$, where ζ is constant. Now, it is worth mentioning that the static solution of the surface density (7) and pressure (8) reduces to

$$\sigma(R_{\rm o}) = \frac{-1}{4\pi R_{\rm o}^2}\left(\sqrt{R_{\rm o}^2 - 2mR_{\rm o}(\zeta+1) + q^2} - \sqrt{R_{\rm o}^2 - 2mR_{\rm o}}\right), \quad (28)$$

$$p(R_{\rm o}) = \frac{1}{8\pi R_{\rm o}^2}\left(\frac{mR_{\rm o}(\zeta+1) - q^2}{\sqrt{R_{\rm o}^2 - 2mR_{\rm o}(\zeta+1) + q^2}} - \frac{mR_{\rm o}}{\sqrt{R_{\rm o}^2 - 2mR_{\rm o}}}\right)$$
$$+ \frac{1}{8\pi R_{\rm o}^2}\left(\sqrt{R_{\rm o}^2 - 2mR_{\rm o}(\zeta+1) + q^2} - \sqrt{R_{\rm o}^2 - 2mR_{\rm o}}\right). \quad (29)$$

Thus, Eq. (21), as expressed in terms of (27), may be found as follows:

$$(R_{\rm o}^2 - mR_{\rm o}(\zeta+1))\sqrt{R_{\rm o}^2 - 2mR_{\rm o}} - (R_{\rm o}^2 - mR_{\rm o})\sqrt{R_{\rm o}^2 - 2mR_{\rm o}(\zeta+1) + q^2}$$
$$+ 2A\left[(R_{\rm o}^2 - 2mR_{\rm o}(\zeta+1) + q^2)\sqrt{R_{\rm o}^2 - 2mR_{\rm o}}\right.$$
$$\left. - (R_{\rm o}^2 - 2mR_{\rm o})\sqrt{R_{\rm o}^2 - 2mR_{\rm o}(\zeta+1) + q^2}\right]$$
$$+2\,(-4\pi)^{\alpha+1}BR_{\rm o}^{2(\alpha+1)-n}\sqrt{R_{\rm o}^2 - 2mR_{\rm o}}\sqrt{R_{\rm o}^2 - 2mR_{\rm o}(\zeta+1) + q^2}$$
$$\times \left[\sqrt{R_{\rm o}^2 - 2mR_{\rm o}(\zeta+1) + q^2} - \sqrt{R_{\rm o}^2 - 2mR_{\rm o}}\right]^{-\alpha} = 0. \quad (30)$$

Equations (26) and (18) can be rearranged to give the following expression:

$$\beta^2 = -\frac{1}{2} - \frac{\chi R^{n+1}\sigma^{\alpha}}{2[(A+1)R^n\sigma^{\alpha+1} - B]} + \frac{R^n}{8[(A+1)R^n\sigma^{\alpha+1} - B][(q^2 - 2mR\zeta)^2 - R^4K]}$$
$$\times \left\{\frac{K}{2\pi^2}\sigma^{\alpha-1}\left[mR(\zeta+2) - \frac{3}{2}q^2\right] + 4\sigma^{\alpha+1}[6m^2R^2\zeta^2 + 5q^4 - 12mRq^2\zeta]\right.$$

$$- 16R^{-n}[(2A+1)R^n\sigma^{\alpha+1} - 2B](mR\zeta - q^2)(2mR\zeta - q^2)$$
$$+ 2R^{-2n}\sigma^{-\alpha-1}[(2A+1)R^n\sigma^{\alpha+1} - 2B]^2[3(q^2 - 2mR\zeta)^2 + KR^4]\Bigg\}, \tag{31}$$

with $K = (16\pi^2R^2)^2\sigma^4$. Let $\beta^2 = 0$, to get

$$\hat{\chi} \equiv 4\chi R\sigma = -4R^{-n}\sigma^{1-\alpha}[(A+1)R^n\sigma^{\alpha+1} - B] + \frac{\sigma^{1-\alpha}}{[(q^2 - 2mR\zeta)^2 - R^4K]}$$
$$\times\left\{\frac{K}{2\pi^2}\sigma^{\alpha-1}\left[mR(\zeta+2) - \frac{3}{2}q^2\right] + 4\sigma^{\alpha+1}[6m^2R^2\zeta^2 + 5q^4 - 12mRq^2\zeta]\right.$$
$$- 16R^{-n}[(2A+1)R^n\sigma^{\alpha+1} - 2B](mR\zeta - q^2)(2mR\zeta - q^2)$$
$$\left.+ 2R^{-2n}\sigma^{-\alpha-1}[(2A+1)R^n\sigma^{\alpha+1} - 2B]^2[3(q^2 - 2mR\zeta)^2 + KR^4]\right\}. \tag{32}$$

Inserting Eqs. (28) and (29) into Eq. (25) leads to

$$\beta^2 = -\frac{1}{2} - \frac{\chi R}{2H} + \frac{1}{2HL[(q^2 - 2mR\zeta)^2 - JR^4]}\left\{\frac{R^2J}{2\pi}\left[mR(\zeta+2) - \frac{3}{2}q^2\right]\right.$$
$$+ \frac{L^2}{4\pi R^2}[6m^2R^2\zeta^2 + 5q^4 - 12mRq^2\zeta] - 4LE(mR\zeta - q^2)(2mR\zeta - q^2)$$
$$\left.+ 2\pi R^2E^2[3(q^2 - 2mR\zeta)^2 + JR^4]\right\}, \tag{33}$$

such that

$$L \equiv 4\pi R^2\sigma = \left(\sqrt{R_{\rm o}^2 - 2mR_{\rm o}} - \sqrt{R_{\rm o}^2 - 2mR_{\rm o}(\zeta+1) + q^2}\right),$$
$$E \equiv \sigma + 2p = \frac{1}{4\pi R_{\rm o}^2}\left(\frac{mR_{\rm o}(\zeta+1) - q^2}{\sqrt{R_{\rm o}^2 - 2mR_{\rm o}(\zeta+1) + q^2}} - \frac{mR_{\rm o}}{\sqrt{R_{\rm o}^2 - 2mR_{\rm o}}}\right),$$
$$H \equiv \sigma + p = \frac{1}{8\pi R^2}(L + 4\pi R^2E), \quad J = \frac{L^4}{R^4} \equiv (16\pi^2R^2)^2\left(\frac{L}{4\pi R^2}\right)^4.$$

Using Eq. (33), as taking $\beta^2 = 0$, we obtain

$$\hat{\chi} \equiv 4R\chi\sigma = -\frac{HL}{\pi R^2} + \frac{1}{[(q^2 - 2mR\zeta)^2 - JR^4]}\left\{\frac{J}{2\pi^2}\left[mR(\zeta+2) - \frac{3}{2}q^2\right]\right.$$
$$+ \frac{L^2}{4\pi^2R^4}[6m^2R^2\zeta^2 + 5q^4 - 12mRq^2\zeta]$$
$$\left.- \frac{4LE}{\pi R^2}(mR\zeta - q^2)(2mR\zeta - q^2) + 2E^2[3(q^2 - 2mR\zeta)^2 + JR^4]\right\}. \tag{34}$$

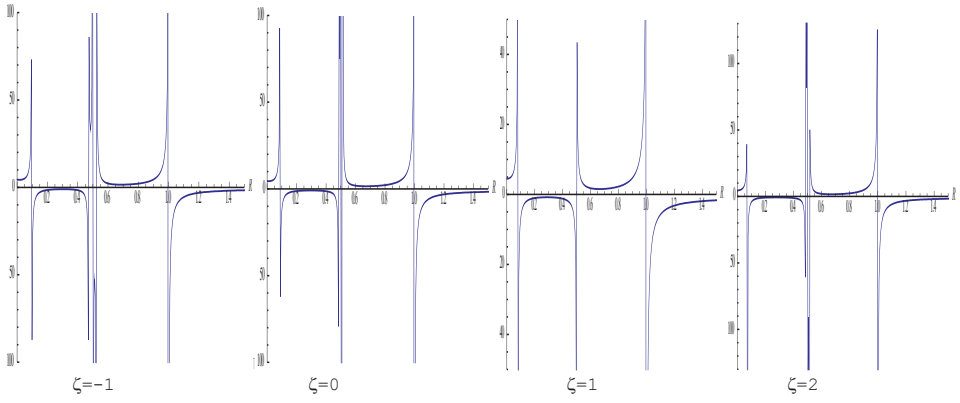

Fig. 1. Stability regions of S-RN ATSW corresponding to $m = 1$, $q = 1$, $n = 1$, $\sigma_{\rm o} = 1$, $\alpha = 1$, $R_{\rm o} = 1$, $A = -0.5$, $B = 0.5$ and $\zeta = -1, 0, 1, 2$ with the fixed value $\chi = 0$.

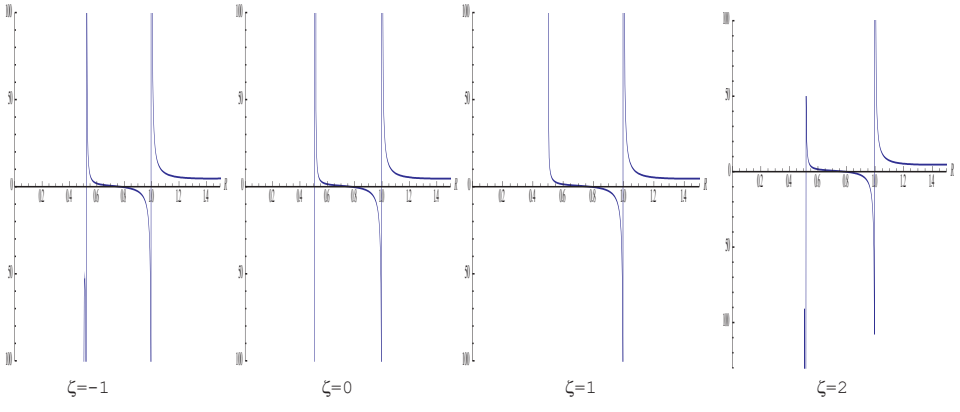

Fig. 2. Stability regions for S-RN ATSW corresponding to $m = 1$, $q = 1$, $n = 1$, $\sigma_{\rm o} = 1$, $\alpha = 1$, $R_{\rm o} = 1$, $A = -0.5$, $B = 0.5$ and $\zeta = -1, 0, 1, 2$ with the fixed value $\chi = -1$.

The effect of variation of β^2 versus R is shown graphically in Figs. 1–4 with taking into consideration different values of m, q, A, B, n, $\sigma_{\rm o}$, α, $R_{\rm o}$, ζ and χ as free parameters.

The effect of variation of $\hat{\chi}$ versus R is plotted in Figs. 5 and 6 taking into consideration different values of m, q, A, B, n, $\sigma_{\rm o}$, α, $R_{\rm o}$ and ζ as free parameters.

The plots of β^2 versus R for an S-RN ATSW are given in Figs. 1–4 for the cases $\chi = 0$, $\chi < 0$ and $\chi > 0$. As illustrated in the following way:

(i) $\chi = 0$ and $\zeta = -1, 0, 1, 2$.

The stable regions for $\zeta = -1$ and $\zeta = 2$ are similar to each other, $\chi = 0$ denotes to MGCG EoS.

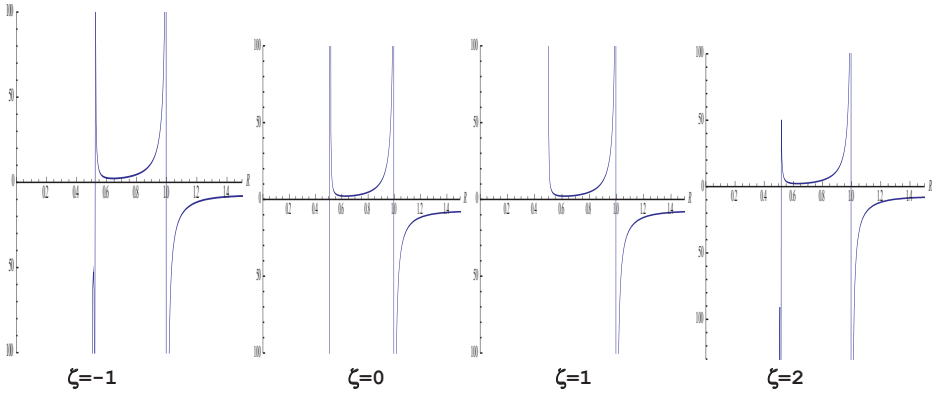

Fig. 3. Stability regions for S-RN ATSW corresponding to $m = 1$, $q = 1$, $n = 1$, $\sigma_o = 1$, $\alpha = 1$, $R_o = 1$, $A = -0.5$, $B = 0.5$ and $\zeta = -1, 0, 1, 2$ with the fixed value $\chi = 1$.

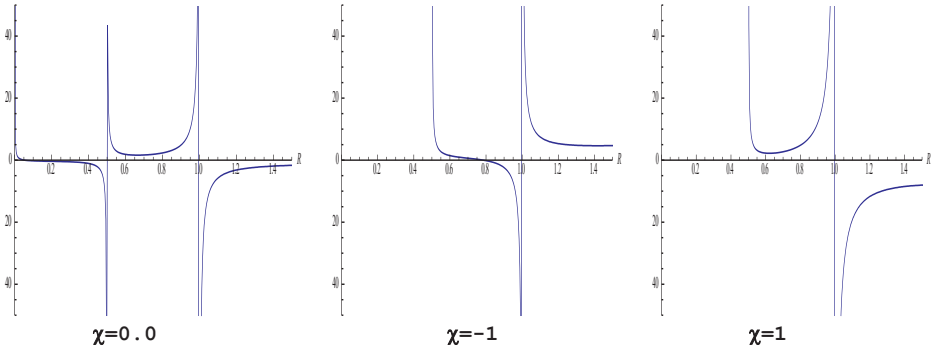

Fig. 4. Stability regions of symmetric S–S TSW corresponding to $m = 1$, $q = 0$, $n = 1$, $\sigma_o = 1$, $\alpha = 1$, $R_o = 1$, $A = -0.5$, $B = 0.5$ and $\chi = 0, -1, 1$ with the fixed value $\zeta = 0$.

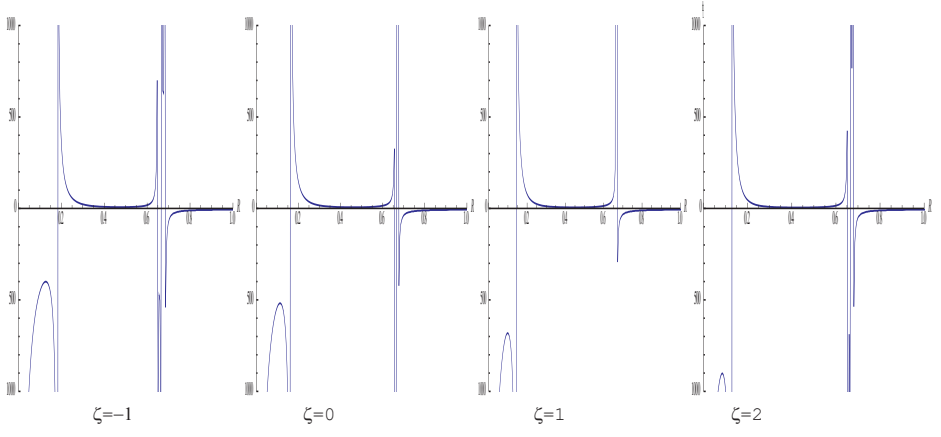

Fig. 5. Stability regions for S-RN ATSW corresponding to $q = 1$, $n = 1$, $\sigma_o = 1$, $\alpha = 1$, $R_o = 1$, $A = -1$, $B = 0.5$ and $\zeta = -1, 0, 1, 2$ with the fixed value $m = 1$.

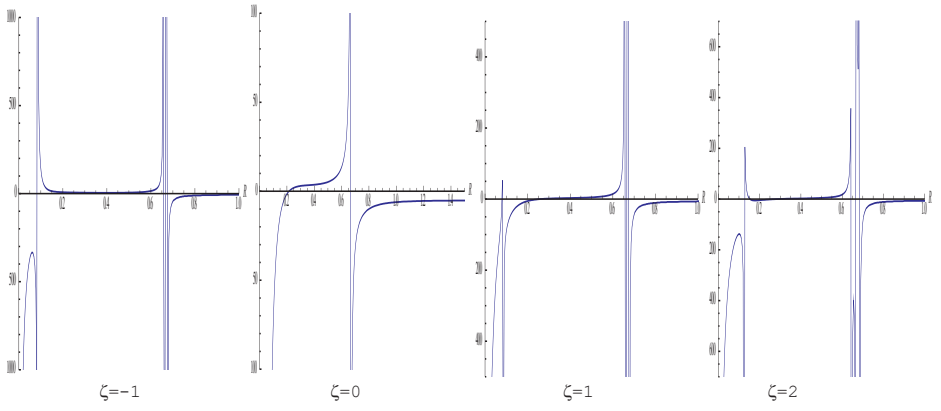

Fig. 6. Stability regions for S–S ATSW corresponding to $m = 1$, $n = 1$, $\sigma_{\rm o} = 1$, $\alpha = 1$, $R_{\rm o} = 1$, $A = -1$, $B = 0.5$ and $\zeta = -1, 0, 1$ with the fixed value $q = 0$.

(ii) $\chi < 0$ and $\zeta = -1, 0, 1, 2$.

Both the range and shape of the plot exhibit notable change with respect to the case of a $\chi = 0$, $\chi > 0$; the stable regions for $\zeta = -1$ and $\zeta = 2$ are similar to each other.

(iii) $\chi > 0$ and $\zeta = -1, 0, 1, 2$.

The plots have changed compared with the case of $\chi = 0$, the shift in the range of β^2 states that the stability regions have decreased; the stable regions for $\zeta = -1$ and $\zeta = 2$ are similar to each other.

When $\zeta = 0$, it gives rise to consider the throat which connects S-RN geometries has the same central mass.

While for $\zeta = 0$ and $q = 0$, one may regard that the symmetry S–S geometries due to the relationship between β^2 and R for $\chi = 0, -1, 1$ are shown in Fig. 4. Moreover, the pressure is a function of radius $\hat{\chi}$, when $\beta^2 = 0$, is given in Fig. 5; the stable regions for $\zeta = -1$ and $\zeta = 2$ are similar to each other. In Fig. 6, the stable region of $\zeta = 0$ and $q = 0$ represents the case of symmetric S–S geometries.

3.2. *For a Reissner–Nordström and Schwarzschild–De Sitter spacetimes*

For the RN spacetime and Schwarzschild–De Sitter (SDS) spacetime, the metric of the line element (1) is given by

$$f_+(r_+) = 1 - \frac{2m_+}{r_+} + \frac{q_+^2}{r_+^2} \quad \text{and} \quad f_-(r_-) = 1 - \frac{2m_-}{r_-} - \xi^2 r_-^2, \tag{35}$$

provided that $\xi^2 = \frac{1}{3}\Lambda$, where Λ is a cosmological constant. In case of RN and SD spacetimes assuming that: $m_- = m$, $m_+ = (1 + \eta)m$ and $q_+ = q$, where η is constant.

Consequently, the static solution of the surface density (7) and pressure (8) becomes

$$\sigma(R_{\rm o}) = \frac{-1}{4\pi R_{\rm o}^2}\left(\sqrt{R_{\rm o}^2 - 2mR_{\rm o}(\eta+1)+q^2} - \sqrt{R_{\rm o}^2 - 2mR_{\rm o} - \xi^2 R^4}\right), \quad (36)$$

$$p(R_{\rm o}) = \frac{1}{8\pi R_{\rm o}^2}\left(\frac{mR_{\rm o}(\eta+1)-q^2}{\sqrt{R_{\rm o}^2 - 2mR_{\rm o}(\eta+1)+q^2}} - \frac{mR_{\rm o} - \xi^2 R^2}{\sqrt{R_{\rm o}^2 - 2mR_{\rm o} - \xi^2 R^4}}\right) + \frac{1}{8\pi R_{\rm o}^2}\left(\sqrt{R_{\rm o}^2 - 2mR_{\rm o}(\eta+1)+q^2} - \sqrt{R_{\rm o}^2 - 2mR_{\rm o} - \xi^2 R^4}\right). \quad (37)$$

Equation (21) in terms of (35) can be rewritten as:

$$\begin{aligned}
&(R_{\rm o}^2 - mR_{\rm o}(\eta+1))\sqrt{R_{\rm o}^2 - 2mR_{\rm o} - \xi^2 R^4} \\
&\quad - (R_{\rm o}^2 - mR_{\rm o} - 2\xi^2 R^4)\sqrt{R_{\rm o}^2 - 2mR_{\rm o}(\eta+1)+q^2} \\
&\quad + 2A\left[(R_{\rm o}^2 - 2mR_{\rm o}(\eta+1)+q^2)\sqrt{R_{\rm o}^2 - 2mR_{\rm o} - \xi^2 R^4}\right. \\
&\quad \left. - (R_{\rm o}^2 - 2mR_{\rm o} - \xi^2 R^4)\sqrt{R_{\rm o}^2 - 2mR_{\rm o}(\eta+1)+q^2}\right] \\
&\quad + 2(-4\pi)^{\alpha+1} B R_{\rm o}^{2(\alpha+1)-n}\sqrt{R_{\rm o}^2 - 2mR_{\rm o} - \xi^2 R^4}\sqrt{R_{\rm o}^2 - 2mR_{\rm o}(\eta+1)+q^2} \\
&\quad \times \left[\sqrt{R_{\rm o}^2 - 2mR_{\rm o}(\eta+1)+q^2} - \sqrt{R_{\rm o}^2 - 2mR_{\rm o} - \xi^2 R^4}\right]^{-\alpha} = 0. \quad (38)
\end{aligned}$$

Using Eq. (18) and rearranging Eq. (26) will lead to

$$\begin{aligned}
\beta^2 = &-\frac{1}{2} - \frac{\chi R^{n+1}\sigma^\alpha}{2[(A+1)R^n\sigma^{\alpha+1} - B]} \\
&+ \frac{R^n}{8[(A+1)R^n\sigma^{\alpha+1} - B][(q^2 - 2mR\eta + \xi^2 R^4)^2 - R^4\tilde{K}]} \\
&\times \left\{\frac{\tilde{K}}{4\pi^2}\sigma^{\alpha-1}[2mR(\zeta+2) - 3q^2 + \xi^2 R^4] + 4\sigma^{\alpha+1}[6m^2R^2\eta^2 + 5q^4\right. \\
&- 12mRq^2\eta - 6R^4q^2\xi^2 + 3\xi^4R^8] - 16R^{-n}[(2A+1)R^n\sigma^{\alpha+1} - 2B] \\
&\times (-2mR\eta + q^2 + \xi^2R^4)(mR\eta - q^2 + \xi^2R^4) + 2R^{-2n}\sigma^{-\alpha-1} \\
&\left.\times [(2A+1)R^n\sigma^{\alpha+1} - 2B]^2[3(-2mR\eta + q^2 + \xi^2R^4)^2 + \tilde{K}R^4]\right\}, \quad (39)
\end{aligned}$$

with $\tilde{K} = (16\pi^2R^2)^2\sigma^4$. Returning to Eq. (39) and letting $\beta^2 = 0$, we will get

$$\begin{aligned}
\hat{\chi} \equiv 4\chi R\sigma = &-4R^{-n}\sigma^{1-\alpha}[(A+1)R^n\sigma^{\alpha+1} - B] + \frac{\sigma^{1-\alpha}}{[(q^2 - 2mR\eta + \xi^2R^4)^2 - R^4\tilde{K}]} \\
&\times \left\{\frac{\tilde{K}}{4\pi^2}\sigma^{\alpha-1}[2mR(\zeta+2) - 3q^2 + \xi^2R^4] + 4\sigma^{\alpha+1}[6m^2R^2\eta^2 + 5q^4 - 12mRq^2\eta\right.
\end{aligned}$$

$$- 6R^4q^2\xi^2 + 3\xi^4R^8] - 16R^{-n}[(2A+1)R^n\sigma^{\alpha+1} - 2B](-2mR\eta + q^2 + \xi^2R^4)$$
$$\times (mR\eta - q^2 + \xi^2R^4) + 2R^{-2n}\sigma^{-\alpha-1}[(2A+1)R^n\sigma^{\alpha+1} - 2B]^2$$
$$\times [3(-2mR\eta + q^2 + \xi^2R^4)^2 + \tilde{K}R^4]\Bigg\}. \tag{40}$$

Plugging Eqs. (28) and (29) into (25) becomes

$$\beta^2 = -\frac{1}{2} - \frac{\chi R}{2\tilde{H}} + \frac{1}{2\tilde{H}\tilde{L}[(-2mR\eta + q^2 + \xi^2R^4)^2 - \tilde{J}R^4]}\Bigg\{\frac{R^2\tilde{J}}{4\pi}[2mR(\eta+2)$$
$$- 3q^2 + \xi^2R^4] + \frac{\tilde{L}^2}{4\pi R^2}[6m^2R^2\eta^2 + 5q^4 - 12mRq^2\eta - 6R^4q^2\xi^2 + 3\xi^4R^8]$$
$$- 4\tilde{L}\tilde{E}(-2mR\eta + q^2 + \xi^2R^4)(mR\eta - q^2 + \xi^2R^4)$$
$$+ 2\pi R^2\tilde{E}^2[3(-2mR\eta + q^2 + \xi^2R^4)^2 + \tilde{J}R^4]\Bigg\} \tag{41}$$

with

$$\tilde{L} \equiv 4\pi R^2\sigma = \left(\sqrt{R_{\rm o}^2 - 2mR_{\rm o}(\eta+1) + q^2} - \sqrt{R_{\rm o}^2 - 2mR_{\rm o} - \xi^2R^4}\right),$$

$$\tilde{E} \equiv \sigma + 2p = \frac{1}{4\pi R_{\rm o}^2}\left(\frac{mR_{\rm o}(\eta+1) - q^2}{\sqrt{R_{\rm o}^2 - 2mR_{\rm o}(\eta+1) + q^2}} - \frac{mR_{\rm o} - \xi^2R^2}{\sqrt{R_{\rm o}^2 - 2mR_{\rm o} - \xi^2R^4}}\right),$$

$$\tilde{H} \equiv \sigma + p = \frac{1}{8\pi R^2}(\tilde{L} + 4\pi R^2\tilde{E}),$$

$$\tilde{J} = \frac{\tilde{L}^4}{R^4} \equiv (16\pi^2R^2)^2\left(\frac{\tilde{L}}{4\pi R^2}\right)^4.$$

Let $\beta^2 = 0$ yield

$$\hat{\chi} \equiv 4R\chi\sigma = -\frac{\tilde{H}\tilde{L}}{\pi R^2} + \frac{1}{[(-2mR\eta + q^2 + \xi^2R^4)^2 - \tilde{J}R^4]}\Bigg\{\frac{\tilde{J}}{4\pi^2}[2mR(\eta+2)$$
$$- 3q^2 + \xi^2R^4] + \frac{\tilde{L}^2}{4\pi R^2}[6m^2R^2\eta^2 + 5q^4 - 12mRq^2\eta - 6R^4q^2\xi^2 + 3\xi^4R^8]$$
$$- \frac{4\tilde{L}\tilde{E}}{\pi R^2}(-2mR\eta + q^2 + \xi^2R^4)(mR\eta - q^2 + \xi^2R^4)$$
$$+ 2\tilde{E}^2[3(-2mR\eta + q^2 + \xi^2R^4)^2 + \tilde{J}R^4]\Bigg\}. \tag{42}$$

Thus, the plots of β^2 versus R are presented in Figs. 7–10, having different values of m, q, A, B, n, $\sigma_{\rm o}$, α, $R_{\rm o}$, ξ, η and χ as free parameters.

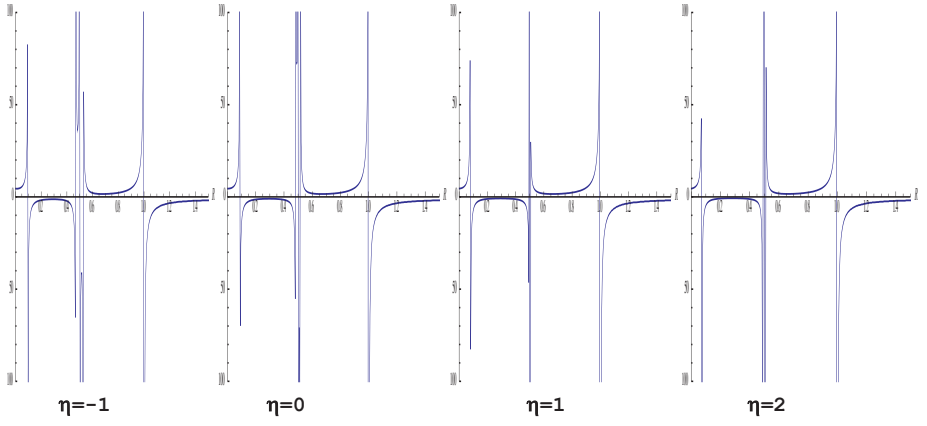

Fig. 7. Stability regions of RN-S De Sitter ATSW corresponding to $m = 1$, $q = 1$, $n = 1$, $\sigma_o = 1$,$\alpha = 1$, $R_o = 1$, $A = -0.5$, $B = 0.5$, $\xi = \pm 2$ and $\eta = -1, 0, 1, 2$ with the fixed value $\chi = 0$.

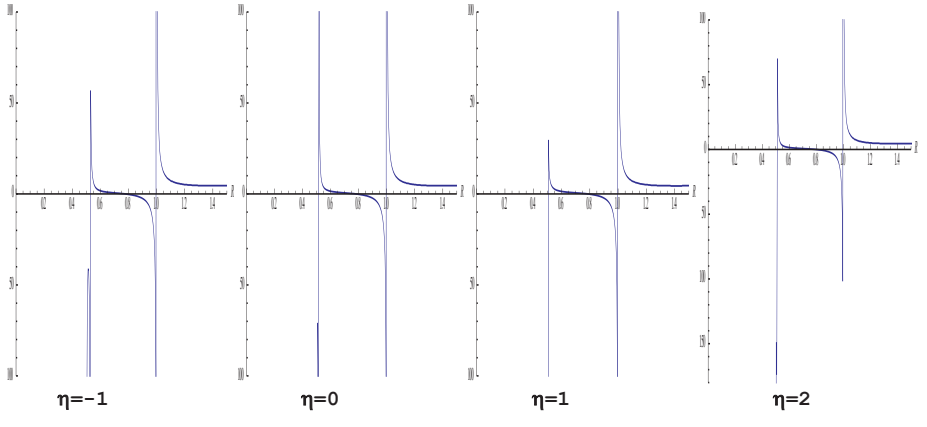

Fig. 8. Stability regions for RN-S De Sitter ATSW corresponding to $m = 1$, $q = 1$, $n = 1$, $\sigma_o = 1$, $\alpha = 1$, $R_o = 1$, $A = -0.5$, $B = 0.5$, $\xi = \pm 2$ and $\eta = -1, 0, 1, 2$ with the fixed value $\chi = -1$.

Thus, the plots of $\hat{\chi}$ versus R are presented in Figs. 11 and 12, having different values of m, q, A, B, n, σ_o, α, R_o, ξ and η as free parameters.

For an RN–SD Sitter ATSW, the plot of β^2 versus R is given in Figs. 7–10 for the cases $\chi = 0$, $\chi < 0$ and $\chi > 0$. As illustrated in the following way:

(i) $\chi = 0$ and $\eta = -1, 0, 1, 2$.

The stable regions for $\eta = -1$ and $\eta = 0$ are similar to each other, also $\eta = 1$ and $\eta = 2$ are similar to each other, $\chi = 0$ denotes to MGCG EoS.

(ii) $\chi < 0$ and $\eta = -1, 0, 1, 2$.

In general, both the range and shape of the plot exhibit notable change with respect to the case of a $\chi = 0$, $\chi > 0$; the stable regions for $\eta = -1, 0$ and $\eta = 2$ are similar to each other.

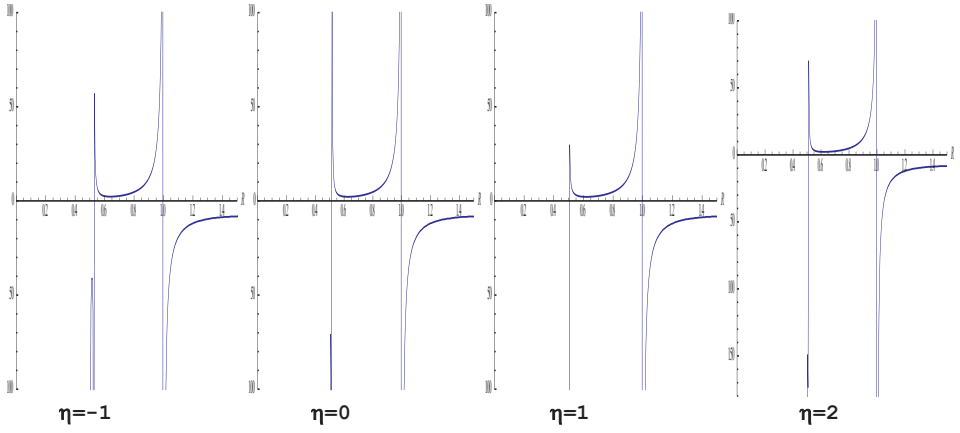

Fig. 9. Stability regions for RN-S De Sitter ATSW corresponding to $m = 1$, $q = 1$, $n = 1$, $\sigma_o = 1$, $\alpha = 1$, $R_o = 1$, $A = -0.5$, $B = 0.5$, $\xi = \pm 2$ and $\eta = -1, 0, 1, 2$ with the fixed value $\chi = 1$.

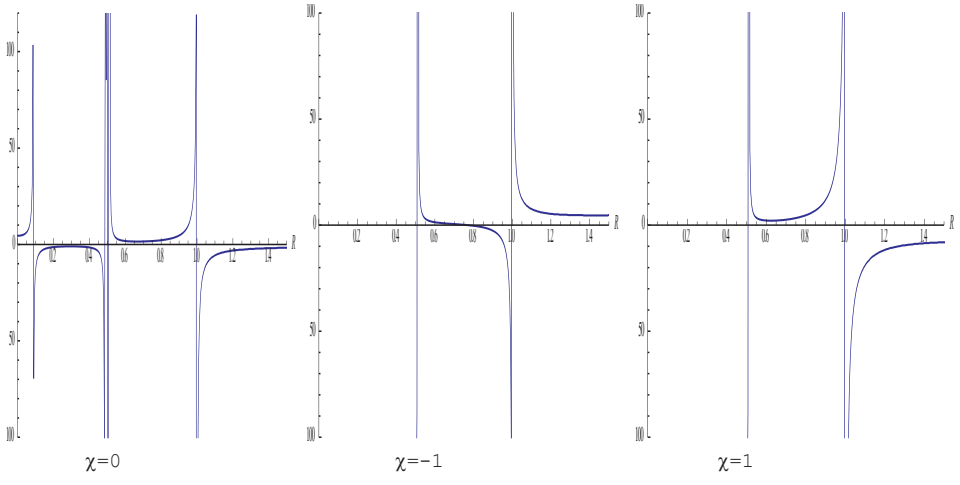

Fig. 10. Stability regions of RN-S ATSW corresponding to $m = 1$, $q = 1$, $n = 1$, $\sigma_o = 1$, $\alpha = 1$, $R_o = 1$, $A = -0.5$, $B = 0.5$, $\xi = 0$ and $\chi = 0, -1, 1$ with the fixed value $\eta = 0$.

(iii) $\chi > 0$ and $\eta = -1, 0, 1, 2$.

The plots have drastic change compared with the case of $\chi = 0$, the shift in the range of β^2 shows that the stability regions have decreased; the stable regions for $\eta = -1, 0$ and $\eta = 2$ are similar to each other.

The cases $\xi = 0$ and $\eta = 0$ denote the RN-S ATSW geometries, the plots of β^2 versus R in Fig. 10 are similar to the graphs of Figs. 1–4 for $\chi = 0, -1, 1$ and $\zeta = 0$.

Further, the pressure is a function of the radius $\hat{\chi}$, when $\beta^2 = 0$, is given in Fig. 11; the stable regions for $\eta = -1$ and $\eta = 0$ are similar to each other.

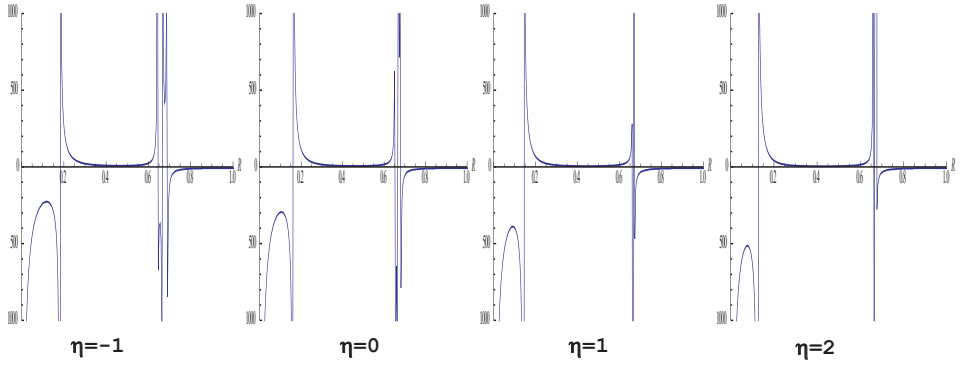

Fig. 11. Stability regions for RN-S De Sitter ATSW corresponding to $m = 1$, $q = 1$, $n = 1$, $\sigma_{\rm o} = 1$, $\alpha = 1$, $R_{\rm o} = 1$, $A = -1$, $B = 0.5$ and $\eta = -1, 0, 1, 2$ with the fixed value $\xi = \pm 2$.

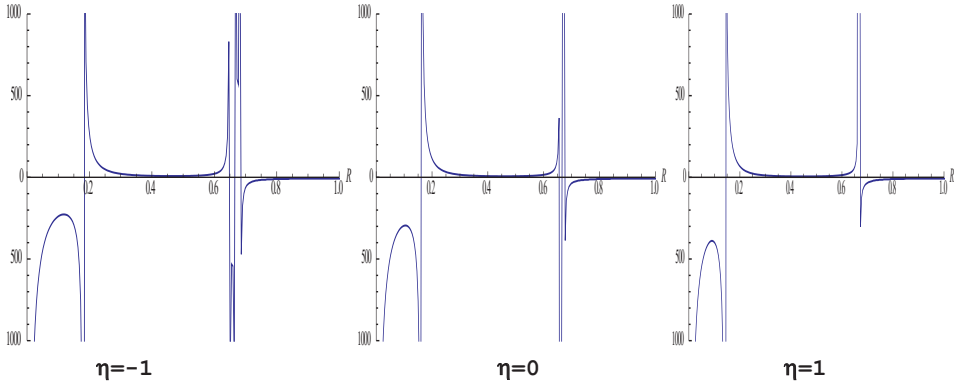

Fig. 12. Stability regions for RN-S ATSW corresponding to $m = 1$, $q = 1$, $n = 1$, $\sigma_{\rm o} = 1$, $\alpha = 1$, $R_{\rm o} = 1$, $A = -1$, $B = 0.5$ and $\eta = -1, 0, 1$ with the fixed value $\xi = 0$.

In Fig. 12, the stable regions of $\xi = 0$ and $\eta = -1, 0, 1$ represent the case of RN-S ATSW geometries, the graphs of Figs. 12 and 5 are similar to each other. Furthermore, for $q = 0$ and $\xi = 0$, the case of symmetric S-S geometries (when $\eta = 0$) is recovered.

From Eqs. (10) and (18), the variation of $V_{\rm eff}$ versus R is plotted in Figs. 13 and 14 with different values of m, q, A, B, n, $\sigma_{\rm o}$, α, $R_{\rm o}$, ζ, ξ and η as free parameters. The stable regions for $\eta = 1$ and $\eta = 2$ are similar to each other. The plots of $V_{\rm eff}$ versus R in both cases (RN-S De Sitter and S-RN ATSWs) are the same.

In the case of $\xi = 0$ and $\eta = 0$ or $\zeta = 0$, Fig. 14(b) denotes the RN-S ATSW geometries and is similar to the graph in Fig. 13 with $\eta = 0$, the plots of $V_{\rm eff}$ versus R in Fig. 14 for both cases (RN-S De Sitter and S-RN ATSWs) are similar. Further, for the case of $\xi = 0$, $q = 0$ and $\eta = 0$ or $\zeta = 0$, Fig. 14(c) denotes the symmetric S–S TSW geometries.

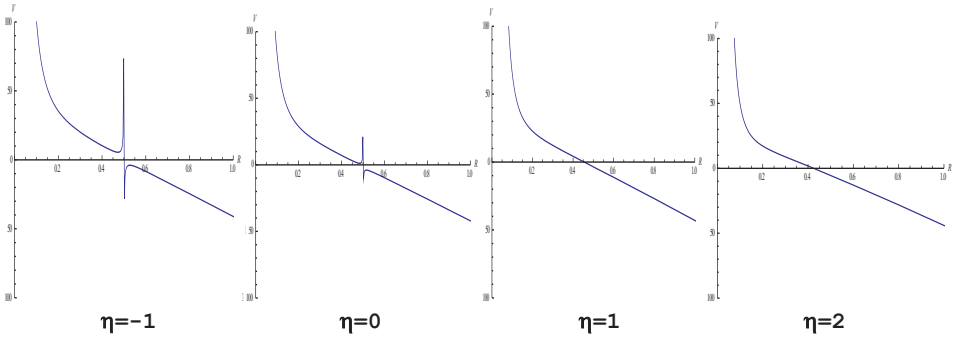

Fig. 13. Stability regions for RN-S De Sitter ATSW corresponding to $m = 1$, $q = 1$, $n = 1$, $\sigma_o = 1$, $R_o = 1$, $\alpha = 1$, $A = -0, 5$, $B = 0.5$ and $\eta = \zeta = -1, 0, 1, 2$ with the fixed value $\xi = \pm 2$.

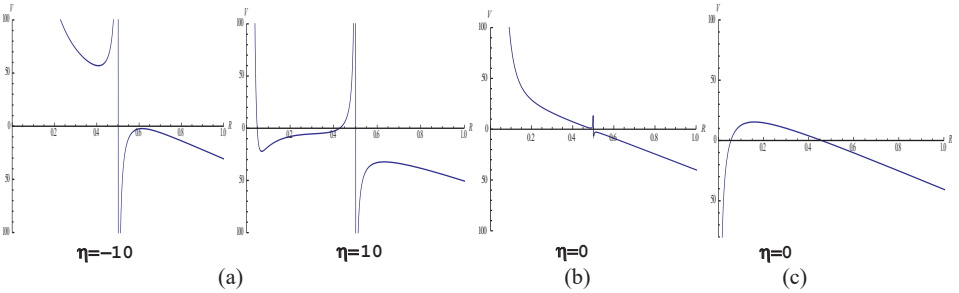

Fig. 14. Stability regions of V_{eff} versus R corresponding to $m = 1$, $n = 1$, $\sigma_o = 1$, $R_o = 1$, $\alpha = 1$, $A = -0, 5$, $B = 0.5$. (a) $q = 1$, $\eta = \zeta = -10, 10$ and $\xi = \pm 2$ denotes to RN-S De Sitter ATSWs, (b) $q = 1$, $\eta = \zeta = 0$ and $\xi = 0$ denotes to RN-S ATSWs, (c) $q = 0$, $\eta = \zeta = 0$ and $\xi = 0$ denotes to symmetric S-S TSWs.

4. Conclusion

It has been sought in several works on stability analysis which have been applied on symmetric TSWs. However, a few types of researches have been discussed on case of the stability of asymmetric TSWs. Yet, such a type stability and the dynamics of ATSWs of two different cases of ATSW connecting two manifolds i.e. the Schwarzschild metric connected to RN spacetimes and the RN metric connected to the Schwarzschild–De Sitter spacetime are discussed.

Accordingly, searching for a specific static solution with a VMGCG has been carried out in such a way that the pressure is considered as a function of both radius and density. Consequently, for a variable EoS, there exist two parameters, the first is $\beta^2 = dp/d\sigma$, the speed of sound and the second is $\chi = -dp/dR$, the dependence of pressure on the throat wormholes radius. Furthermore, the stability of these two cases of ATSWs with two parameters β^2 and χ is expressed as the solution of ATSW. It may give that the system is stable at $V''(R_o) > 0$, while it turns out to be unstable at $V''(R_o) < 0$. This may emphasize that the stability may be affected to a great extent by parameter χ. Moreover, in case of a variable

EoS, the existence of pressure radial dependency χ affects the stability regions of ATSWs.

By graphing their stability analysis diagrams in both cases, the existence of stable/unstable regions depends on the choice of the suitable values of parameters. Meanwhile, the stability regions have been plotted in Figs. 1–4 and 7–10 in the form of parameter β^2 versus R in the two specific cases. In addition, the stability regions have been plotted in Figs. 5 and 10 in the form of parameter χ versus R in the two specific cases, provided that the stability regions are extended by χ. We eventually figure out that the existence of parameters β^2 and χ is affected with the stability region of ATSWs, where it can be shown as the effective potential of ATSWs as plotted in Figs. 13 and 14, respectively.

Acknowledgment

I would like to thank Prof. M. Kahil, MSA University for his helpful reviewing of the English language.

References

1. W. Israel, *Nuovo Cimento B* **44**, 1 (1966).
2. M. S. Morris and K. S. Thorne, *Am. J. Phys.* **56**, 395 (1988).
3. M. Visser, *Lorentzian Wormholes*: *From Einstein to Hawking* (AIP, 1995).
4. M. Visser, *Phys. Rev. D* **39**, 3182 (1989).
5. E. F. Eiroa, *Phys. Rev. D* **80**, 044033 (2009).
6. E. Poisson and M. Visser, *Phys. Rev. D* **52**, 7318 (1995).
7. N. M. Garica, F. S. N. Lobo and M. Visser, *Phys Rev. D* **86**, 044026 (2012).
8. S. H. Mazharimousavi, M. Halilsoy and Z. Amirabi, *Phys. Rev. D* **89**, 084003 (2014).
9. S. H. Mazharimousavi, M. Halilsoy and S. N. H. Amen, *Int. J. Mod. Phys. D* **26**, 1750158 (2017).
10. V. Varela, *Phys. Rev. D* **92**, 044002 (2015).
11. V. A. Eid, *Astrophys. Space. Sci.* **15**, 203 (2013).
12. V. M. Sharif and M. Azam, *Chinese Phys. B* **22**, 050401 (2013).
13. V. E. F. Eiroa and C. Simeone, *Phys. Rev. D* **70**, 044008 (2004).
14. V. A. Eid, *Eur. Phys. J. Plus* **131**, 298 (2016).
15. V. M. C. Bento, O. Bertolami and A. A. Sen, *Phys. Rev. D* **66**, 043507 (2002).
16. V. F. S. N. Lobo, *Phys. Rev. D* **73**, 064028 (2006).
17. V. R. Caldwell, R. Dave and P. J. Steinhardt, *Phys. Rev. Lett.* **80**, 1582 (1998).
18. V. A. A. Sen, S. Sen and S. Sethi, *Phys. Rev. D* **63**, 107501 (2001).
19. V. M. Malguarti, E. J. Copeland and A. R. Liddle, *Phys. Rev. D* **68**, 023512 (2003).
20. V. M. Jamil, *Nuovo Cimento B* **123**, 599 (2008).
21. D. Wang and X. Meng, *Phys. Dark Universe* **17**, 46 (2017).
22. S. D. Forghani, S. H. Mazharimousavi and M. Halilsoy, *Eur. Phys. J. C* **78**, 469 (2018).
23. S. D. Forghani, S. H. Mazharimousavi and M. Halilsoy, *Eur. Phys. J. Plus* **133**, 497 (2018).
24. S. D. Forghani, S. H. Mazharimousavi and M. Halilsoy, *Eur. Phys. J. Plus* **134**, 342 (2019).
25. S. D. Forghani, S. H. Mazharimousavi and M. Halilsoy, *J. Cosmol. Astropart. Phys.* **10**, 067 (2019).